Experiments in Fluids (2005)
DOI 10.1007/s00348-005-0089-2

RESEARCH ARTICLE

T. Nakano · N. Fujisawa · S. Lee

Measurement of tonal-noise characteristics and periodic flow structure around NACA0018 airfoil

Received: 17 June 2005 / Revised: 10 November 2005 / Accepted: 10 November 2005

Abstract The characteristics of tonal noise and the variations of flow structure around NACA0018 airfoil in a uniform flow are studied by means of simultaneous measurement of noise and velocity field by particle-image velocimetry to understand the generation mechanism of tonal noise. Measurements are made on the noise characteristics, the phase-averaged velocity field with respect to the noise signal, and the cross-correlation contour of velocity fluctuations and noise signal. These experimental results indicate that the tonal noise is generated from the periodic vortex structure on the pressure surface of the airfoil near the trailing edge of the airfoil. It is found that the vortex structure is highly correlated with the noise signal, which indicates the presence of noise-source distribution on the pressure surface. The vorticity distribution on the pressure surface breaks down near the trailing edge of the airfoil and forms a staggered vortex street in the wake of the airfoil.

1 Introduction

Tonal noise has been generated from an airfoil inclined at small attack angles to the free-stream and at moderate Reynolds numbers. This piercing sound is so strong that the mechanism of noise generation and its control have been a topic of interest in recent years. Since the pioneering work by Paterson et al. (1973), tonal noise has been studied in various types of turbo-machineries (Wright 1976; Longhouse 1977) and the noise spectra and the flow over the airfoil have been examined to explore the mechanism of tonal noise from the airfoil (Tam 1974; Arbey and Bataille 1983; Akishita 1986; Hayashi et al. 1995). These results indicate that tonal noise can be emitted from the self-excited feedback-loop formed by an acoustic field, the boundary layer and the wake of the airfoil. Later, the velocity measurement of the flow over NACA0012 airfoil is carried out by using laser Doppler velocimetry and the generation mechanism of tonal noise is considered in relation to the Tollmien–Schlichting type instability in the separating shear layer over the pressure surface of the airfoil (Nash et al. 1999; McAlpine et al. 1999). More recently, experimental and numerical studies were conducted on the trailing edge noise (Manoha et al. 2000; Wang and Moin 2000; Roger and Moreau 2004). For the theory of trailing edge noise, see the review paper by Howe (1978). However, there is still lack of evidence of a physical mechanism leading to tonal noise generation; so the structure of the boundary layer and the wake of the airfoil should be studied in greater detail.

In order to understand the flow mechanism, velocity measurement by particle-image velocimetry (PIV) provides very useful information on the flow field around an airfoil, which allows for the evaluation of the spatial distribution of the instantaneous velocity and vorticity field (Shih et al. 1995; Kompenhans et al. 2000). However, fewer studies have been reported on the flow field for application to the study on tonal noise mechanism from an airfoil. According to the experiments on a NACA0018 airfoil, the vortex shedding in the wake and the structure of the boundary layer on the airfoil surface near the trailing edge have been studied by the flow visualization and PIV measurement at the condition of tonal noise generation (Nakano et al. 2002; Tomimatsu and Fujisawa 2002) and the results are compared with the numerical simulation (Kim et al. 2005). However, the relationship between the noise and the spatial

T. Nakano · N. Fujisawa (✉)
Department Mechanical Engineering, Niigata University,
8050 Ikarashi 2, 950-2181 Niigata, Japan
E-mail: fujisawa@eng.niigata-u.ac.jp
Tel.: +81-25-2626726
Fax: +81-25-2626726

S. Lee
Department Mechanical Engineering, Inha University,
253 Yonghyun-Dong, Nam-Ku, 402-751 Incheon, Korea

structure of velocity field has not been fully investigated, in spite of its importance for understanding the tonal noise mechanism.

The purpose of this paper is to study the characteristics of tonal noise, the spatial structure of velocity and vorticity field on the boundary layer, and the wake flow of the NACA0018 airfoil by simultaneous measurement of velocity and noise signal. The tonal noise is measured by using a microphone and the structure of velocity and vorticity field with respect to the noise signal is characterized by the phase-averaged PIV measurement and the cross-correlation contour of velocity and noise signal.

2 Main features of flow field

The separation and reattachment points on a NACA0018 airfoil in a uniform flow at various attack angles were given in Table 1, where X_s/C and X_r/C denote the separation and reattachment points, respectively, which are normarized distance by the chord length C of the airfoil. Note that X denotes the distance along the chord measured from the airfoil axis, so that the leading edge and trailing edge of the airfoil corresponds to X/C = -0.3 and $X/C = 0.7$, respectively. The experimental result was taken from the surface flow visualization by liquid crystal coating and the experiment was conducted at Reynolds number $Re = 1.6\times10^5$ in wind tunnel by Nakano et al. (2002). Due to the particularly thick airfoil at low Reynolds number, the laminar boundary layer over the airfoil at 0° separates on the mid region and reattaches on the rear side of the airfoil. The laminar boundary layers on the airfoil separate and become turbulent in the downstream of the reattachment point. When an attack angle increases to 3°, the separation and reattachment points move upward on the suction surface and then move downward along the pressure surface. The movement of the separation and reattachment points is further intensified at 6° and the reattachment point on the pressure surface reaches the trailing edge of the airfoil at this attack angle. With further increase in attack angle to 9°, the separation and reattachment points move further upstream on the suction surface, while the attached flow prevails over the most of the pressure surface and the separation appears near the rear side of the airfoil without reattachment. Further details of flow characteristics can be seen in Nakano et al. (2002).

Table 1 Separation and reattachment points on NACA0018 airfoil

	$\alpha = 0°$	$\alpha = 3°$	$\alpha = 6°$	$\alpha = 9°$
Separation point (X_s/C)				
S.S	0.21	0.07	-0.10	-0.17
P.S.		0.31	0.41	0.53
Reattachment point (X_r/C)				
S.S.	0.52	0.34	0.14	-0.01
P.S.		0.65	0.69	–

3 Experimental apparatus and procedure

3.1 Experimental setup

Figure 1 shows the two-dimensional model of the NACA0018 airfoil in the present experiment, which has chord length $C = 80$ mm and spanwise length 190 mm. The airfoil made of acrylic-resin material is located horizontally at the central plane of the test section. The attack angle of the airfoil is changed by rotating the airfoil about the axis, which is $0.3C$ from the leading edge of the airfoil. The experiments are carried out using an acoustic wind tunnel having a test section of cross-sectional area of 190×190 and 1,000 mm^3 long, which has been described by Tomimatsu and Fujisawa (2002). The contraction ratio of the nozzle is 10, the total number of gids is 6 and the two honeycombs are located inside the wind tunnel. The fan noise is reduced by a reactive type silencer located downstream of the fan and the sound absorber material inside the wind tunnel. The free-stream turbulence intensity is less than 1% and the non-uniformity of the flow is less than 1% of the free-stream velocity.

Figure 2 shows the experimental test section and the measuring system for the present study. The top and bottom of the test section is made of glass-wool material of 25 mm thickness to remove the acoustic resonance, while the side planes are made transparent for flow visualization purpose. The aerodynamic noise is measured by microphones of 0.5 in., which are located on the top and the bottom wall of the test section. The microphone has flat frequency response up to 8 kHz. The output voltage is digitized by an AD converter and is processed in a computer for further signal analysis. The experiments are carried out at free-stream velocity $U_0 = 30$ m/s, which corresponds to the Reynolds number $Re(= U_0C/v) = 1.6\times10^5$ (v kinematic viscosity of fluid).

3.2 Phase-averaged PIV measurement

The phase-averaged velocity field with respect to the noise signal is measured by PIV system, which is illustrated in Fig. 2. The PIV system consists of Nd:YAG lasers (50 mJ), a monochrome CCD camera with frame straddling function (spatial resolution 1,280×1,024 pixels with 12 bits in gray level), and a pulse generator. The frame rate of the CCD camera is 4 frame/s. For the flow visualization study, the smoke is injected from the smoke generator at the air supply inlet of the fan, which allows for uniform spatial distribution of smoke particles in the test section. The diameter of the smoke is about 1 μm. A light sheet illumination is provided from the Nd:YAG lasers to visualize the two-dimensional cross-section of the target image having an area of 30×24 mm^2 near the trailing edge of the airfoil. Thus, the spatial resolution of the image is 23 μm/pixel. The mirror optics located downstream of the airfoil allow the

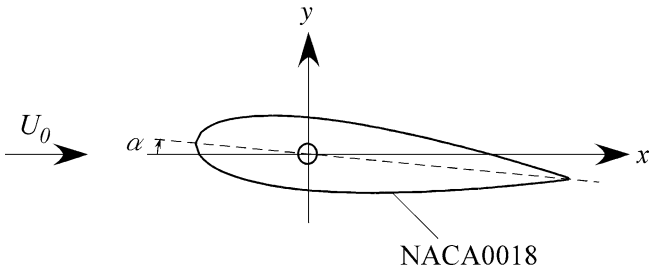

Fig. 1 NACA0018 airfoil

illumination of the target area without shading. The synchronous observation with respect to the pulse illumination of Nd:YAG lasers is made by the monochrome CCD camera in combination with the pulse generator. The time interval between the two sequential images is set to 3 μs . The telecentric lens is used for the imaging to minimize the image distortion by the influence of viewing angles.

Figure 3 shows the time chart of PIV measurement with respect to the microphone signal. When the initial pulse signal triggers the system, the data sampling of the microphone signal starts and the sampled data are digitized for a certain period of time (= 2 ms). Note that the microphone sampling continues until a PIV capture is triggered. The following pulse signals drive the laser and camera for image acquisition. The sampling rate of the signal by AD converter is set to 2 μs in the present experiment, which is due to a short width of the pulse to be detected. Note that the noise signal was band-pass filtered at the tonal noise frequency to remove the background noise, but it is only for the phase determination in PIV measurement. The band-pass filter has one-third octave bandwidth and the phase lag at the setting frequency 2 kHz is negligibly small. The images are captured through a frame grabber during the data sampling of the noise signal. By analyzing the periodicity of microphone signal, the instant of imaging is estimated

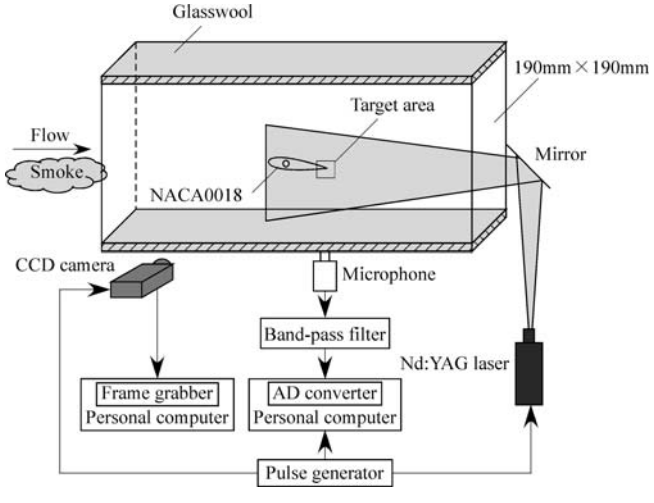

Fig. 2 Experimental setup

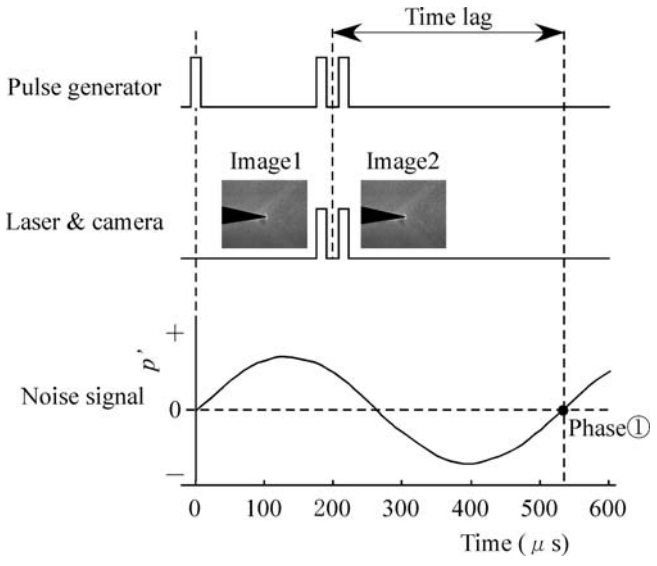

Fig. 3 Time chart of PIV measurement

from the trace of noise signal. Note that the time lag of the sound signal transmitting the distance between the trailing edge of the airfoil and the microphone is corrected in the analysis, which results in the phase-averaged velocity field independent of the location of microphone. In the present experiment, the microphone is placed at $x = 60$ mm on the bottom surface of the test section. The instantaneous velocity field is evaluated from the sequential two images by PIV analysis. Thus, the velocity field at a certain phase of the microphone signal can be evaluated from the present measurement. The phase-averaged velocity field is obtained by averaging 4,000 instantaneous velocity fields at the condition that phase angle agrees with the predetermined phase angle within ±5°. Each phase-averaged velocity field consists of at least 50 instantaneous velocity data. Note that the phase angle of the signal was determined by the zero crossing and the sinusoidal fitting to the signal data.

The PIV analysis is carried out using a gray-level difference method for the cross-correlation calculation between the sequential two images (Fujisawa and Takeda 2003). In the region apart from the solid boundary, the interrogation window is set to 31×31 pixels and the candidate region is searched in the area 45×45 pixels in horizontal and vertical directions. In the region close to the solid boundary, the boundary-fitted interrogation window having an elongated area size was used for the analysis to minimize the erroneous velocity vectors arising from the insufficient tracer particles in the interrogation window near the solid boundary (Fujisawa et al. 2005). The interrogation window is advanced with an overlapped area of 50% in the PIV processing. The sub-pixel interpolation with Gaussian-peak-fitting is incorporated into the analysis to improve the accuracy of velocity measurement. The uncertainty of velocity measurement is estimated to be 3% with 95% coverage, which is obtained from the uncertainty analysis by Fujisawa and Hashizume (2001).

3.3 Measurement of cross-correlation contour of velocity and noise signal

It is very interesting to evaluate the cross-correlation between the fluctuating velocity and the noise signal to understand the noise source in the flow field. Therefore, the cross-correlation coefficients $R_{up}(=\overline{u'p'}/u_{rms}\times p_{rms})$ and $R_{vp}(=\overline{v'p'}/v_{rms}\times p_{rms})$ are calculated from the simultaneous measurement of velocity and noise signal, using the PIV image data and a microphone signal, where u' and v' are streamwise and normal velocity fluctuations, respectively, and p' is a noise signal fluctuation. Note that the microphone is located at $x=60$ mm on the bottom surface of the test section and the flight time of sound was corrected to meet with the sound source at the trailing edge of the airfoil. In this experiment, the PIV measurement is conducted at 4 frame/s and 300 instantaneous velocity fields are measured for the analysis. The number of PIV measurement was found to be enough for the time averaging procedure.

4 Results and discussion

4.1 Measurement of tonal noise

Figures 4 and 5 show the sound pressure level and the sound spectrum, respectively, measured at various attack angles of the airfoil, which are detected by the microphone placed on the top and bottom surfaces of the wind tunnel at the airfoil axis ($x=0$ mm). It is found in Fig. 4 that the sound pressure levels measured on the top and bottom surfaces of the wind tunnel agree within an experimental uncertainty. They increase suddenly at small attack angles of 3°–6° and decrease at further large attack angles. The increase in sound pressure level is found to be due to the appearance of discrete tone noise having a peak frequency at 2.0 kHz as seen in the sound spectrum in Fig. 5. Note that the sound spectra measured on the top and bottom of the wind tunnel agree closely with each other. The secondary peak is also observed in the spectrum at double frequency, though the magnitude is smaller than the primary peak. It should be mentioned that the discrete tone marginally appears at $\alpha=0°$ in the sound spectrum, so that the sound pressure level at zero attack angle is even larger than that of the higher attack angles than 9°. These results indicate that the tonal noise is clearly generated from the airfoil at small attack angles 3° and 6° and it is largest at 6° in the present experiment. It is confirmed that these noise spectra do not change even if the three of four side-walls of the test section are treated by acoustic foams.

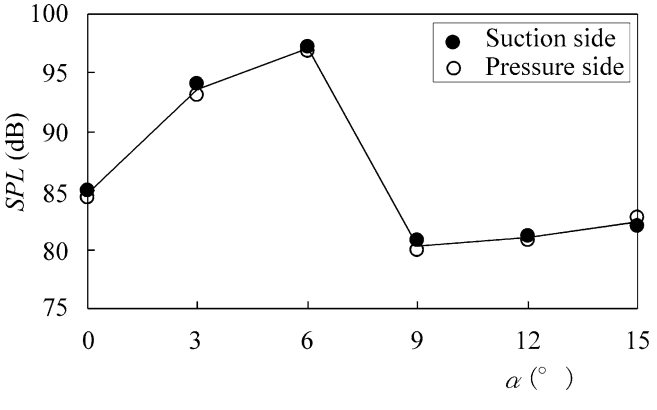

Fig. 4 Sound pressure level with respect to attack angles

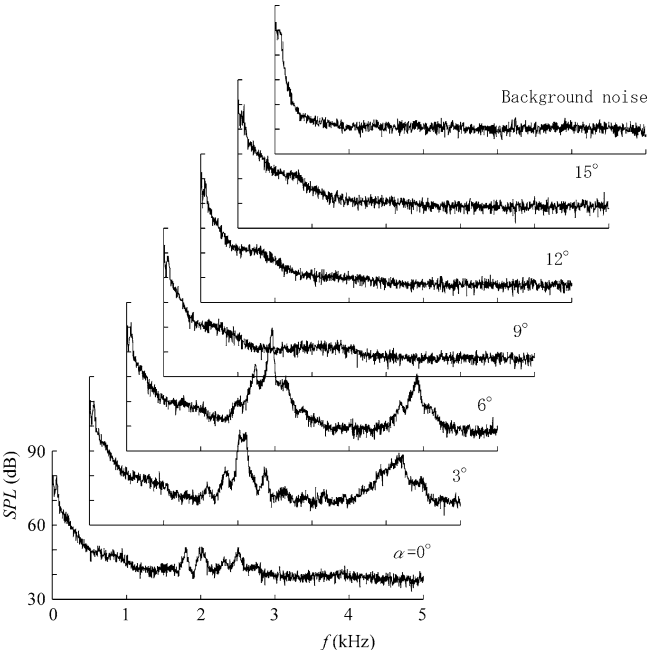

Fig. 5 Sound spectrum at various attack angles

4.2 Phase-averaged PIV measurement

Figure 6a–d shows a typical result of phase-averaged flow field with respect to the noise signal near the trailing edge of the airfoil at attack angle 6°, where the highest peak is observed in the noise spectrum. It gives the velocity vector map (Fig. 6a), the contour of vorticity (Fig. 6b), and the magnified view of streamlines near the trailing edge (Fig. 6c) at various phase angles of the noise signal numbered by 1, 2, 3, and 4, which are shown in Fig. 6d. Here, the velocity magnitude is defined by $\sqrt{u^2+v^2}/U_0$ and the vorticity by $\zeta=C/U_0(\partial V/\partial x-\partial U/\partial y)$. Note that the vorticity is obtained from the circulation method (Raffel et al. 1998).

The contour of velocity field shows the wavy structure in the downstream of the airfoil (Fig. 6a). In the phase 1, the low velocity region prevails over the pressure surface of the airfoil due to the formation of separation region on the rear side of the airfoil, while the flow on the suction surface is fully attached to the airfoil.

Detail examination of the streamlines on the pressure surface of the airfoil (Fig. 6c) shows that the reverse flow appears near the trailing edge of the airfoil and the streamlines direct upward in the downstream of the airfoil. This is followed by the downwash motion in the downstream, which suggests that the vortex streets are formed in the wake of the airfoil. It is also found that the positive vorticity is distributed along the separating-shear-layer on the pressure surface and breaks down near the trailing edge of the airfoil at $X/C=0.67$ (Fig. 6b). The positive vorticity is about to be shed near the trailing edge of the airfoil. The trace of positive vorticity is also found at $X/C=0.82$ in the further downstream, showing the periodicity of vortex shedding from the pressure surface of the airfoil. It is seen that the positive vorticity is generated from the pressure surface and the negative one is shed from the suction surface, which results in a formation of staggered vortices in the

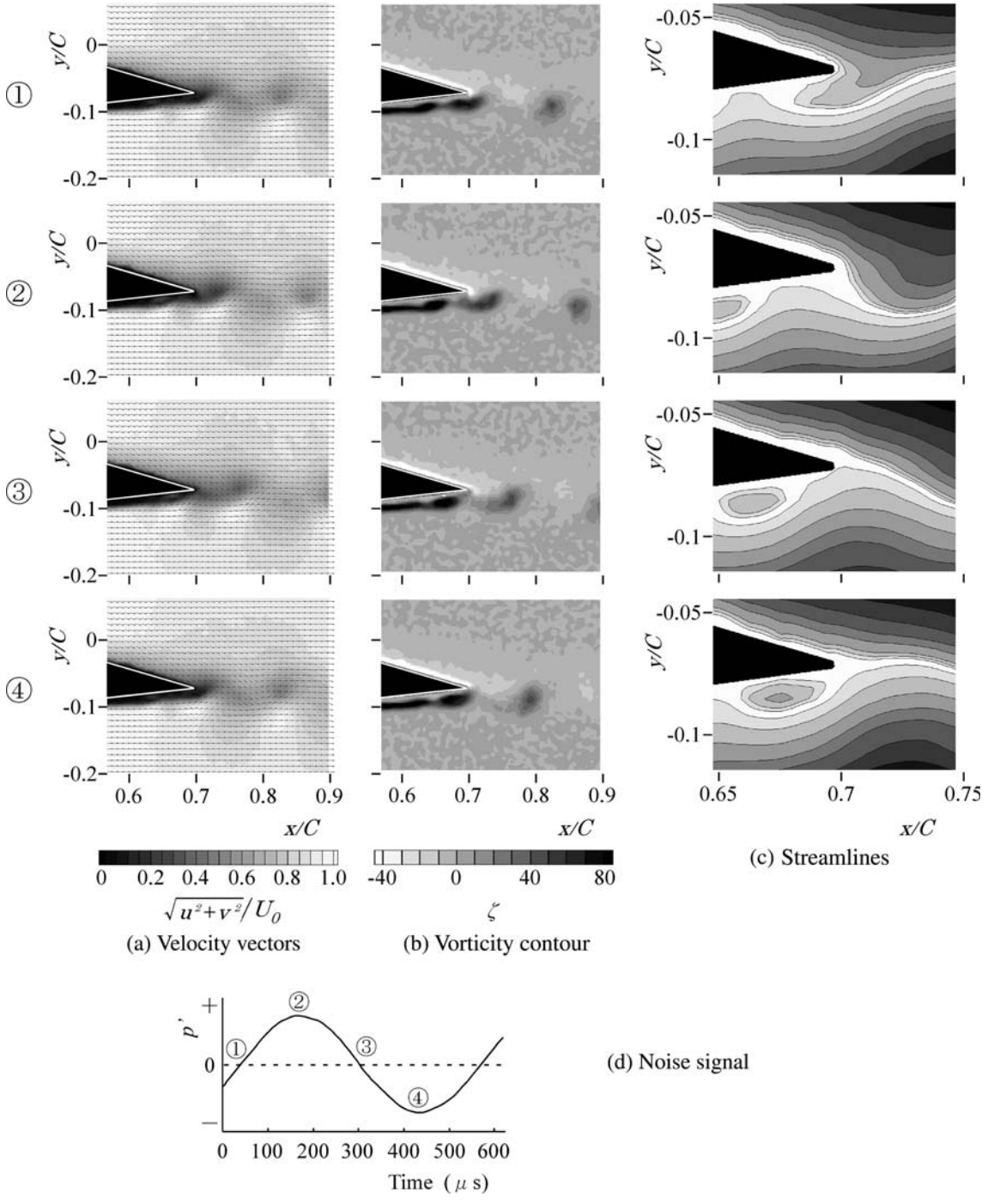

Fig. 6 Phase-averaged velocity and vorticity field at attack angle 6°: **a** Velocity vectors, **b** Vorticity contour, **c** Streamlines, **d** Noise signal

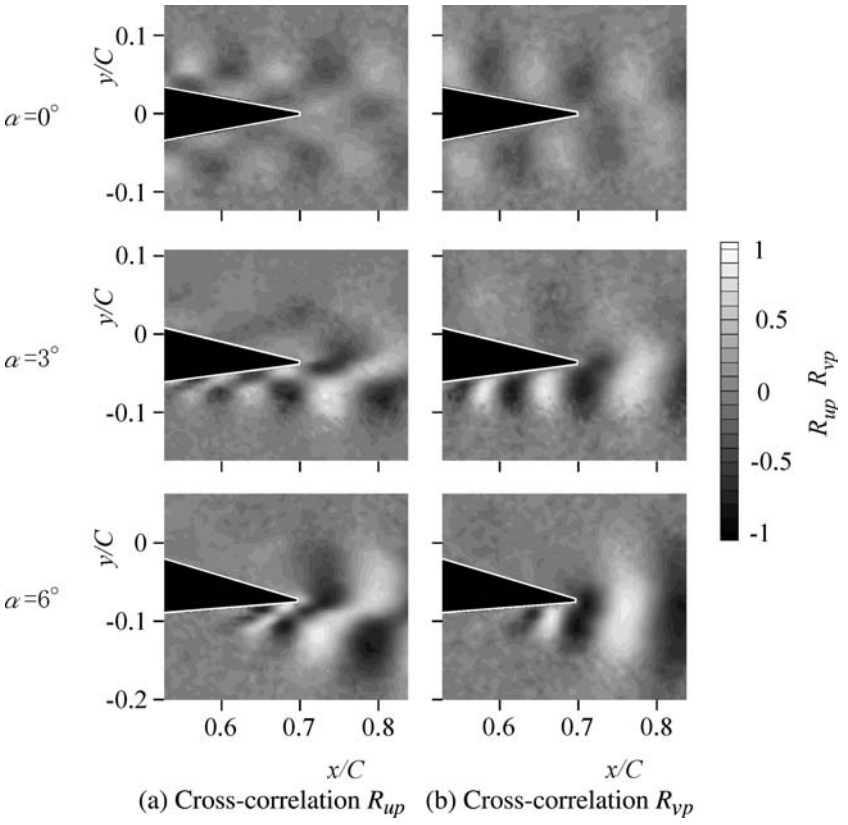

Fig. 7 Cross-correlation contour of velocity fluctuation and noise signal: **a** Cross-correlation R_{up}, **b** Cross-correlation R_{vp}

downstream. However, the magnitude of the positive vorticity is much larger than that of the negative one, suggesting the greater influence of separating shear-layer from the pressure surface on the formation of vortex streets in the wake. It is found that the spacing of the vortices is $s/C = 0.15$ and the convection velocity of the vortices is $0.8\ U_0$.

With an increase in phase angle to the following phase 2, the separation region on the pressure surface spreads into the wake of the airfoil. Then, the isolated vorticity sheds into the wake and all the vortices move further downstream in the wake. In this phase, the downwash motion from the suction surface is magnified and the upwash motion from the pressure surface is weakened near the trailing edge of the airfoil. Note that a newly developed separation region appears on the pressure surface of the airfoil at $X/C = 0.65$, as seen in the magnified view of streamlines near the trailing edge (Fig. 6c). In the following phases 3 and 4, the separation region on the pressure surface moves downstream and the isolated vorticity shifts further downstream. It is seen that the vorticity distribution breaks down around $X/C = 0.65$ and a newly isolated vorticity is about to be shed on the pressure surface at the phases 3 and 4. Corresponding to this change in the flow field, the upwash motion from the pressure surface to the downstream is just started near the trailing edge of the airfoil at the phase 3 and this motion is magnified in the following phase 4.

These results indicate that the periodical oscillation of the velocity field with respect to the noise signal appears in the separation region on the pressure surface and is amplified by approaching the trailing edge of the airfoil, which is followed by the upwash and downwash motion in the downstream of the airfoil. It is clearly seen that such periodicity of the flow field is synchronous with the variation of the tonal noise observed by the microphone. Therefore, the tonal noise is generated from the periodical vortex structure on the pressure surface near the trailing edge of the airfoil. It is expected that a fraction of the kinetic energy of the vortical spots is converted into a sound to fullfil the Kutta condition at this geometrical singularity (Roger and Moreau 2004).

4.3 Correlation contour of fluctuating velocity and noise signal

Figure 7a, b shows the contour of cross-correlation R_{up} and R_{vp} near the trailing edge of the airfoil, respectively, at three attack angles 0°, 3°, and 6°. Note that the tonal noise is marginally observed at zero attack angle and is clearly observed at 3° and 6°, as seen in the sound spectrum in Fig. 5. Reflecting the noise spectrum at zero attack angle, the cross-correlation contour R_{up} is almost uniform in the target area. On the contrary, the cross-correlation contour R_{up} shows a clear periodical structure at attack angles 3° and 6° especially on the pressure surface of the airfoil. The cross-correlation contour at 3° shows the presence of periodical structure near the pressure surface and apart from the surface. It is found

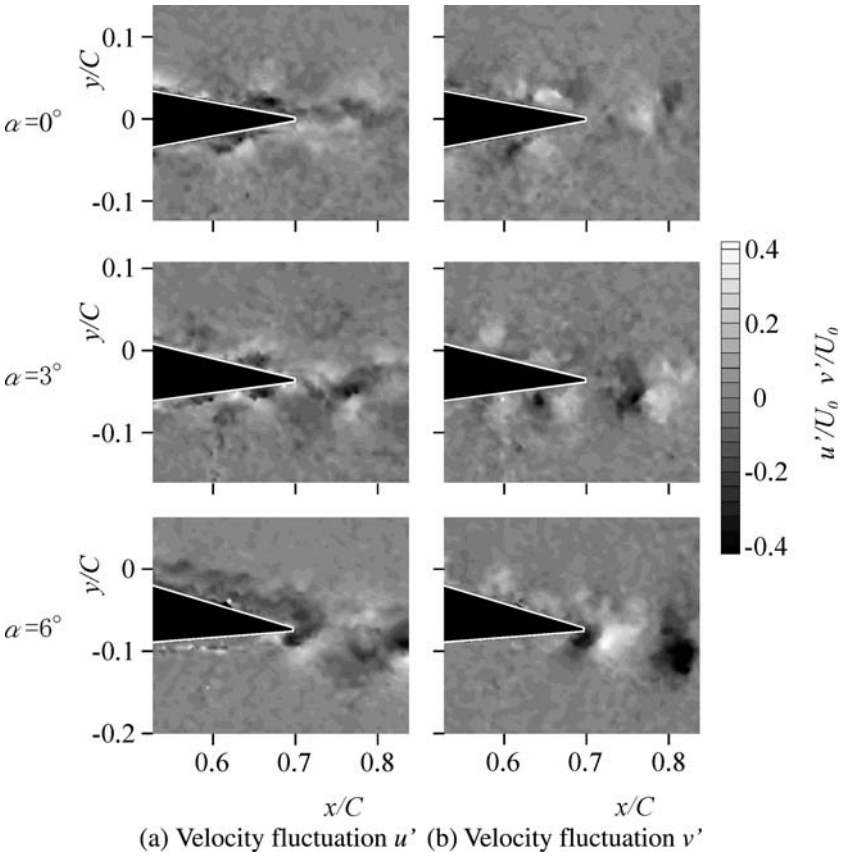

Fig. 8 Contour map of velocity fluctuations: **a** Velocity fluctuation u', **b** Velocity fluctuation v'

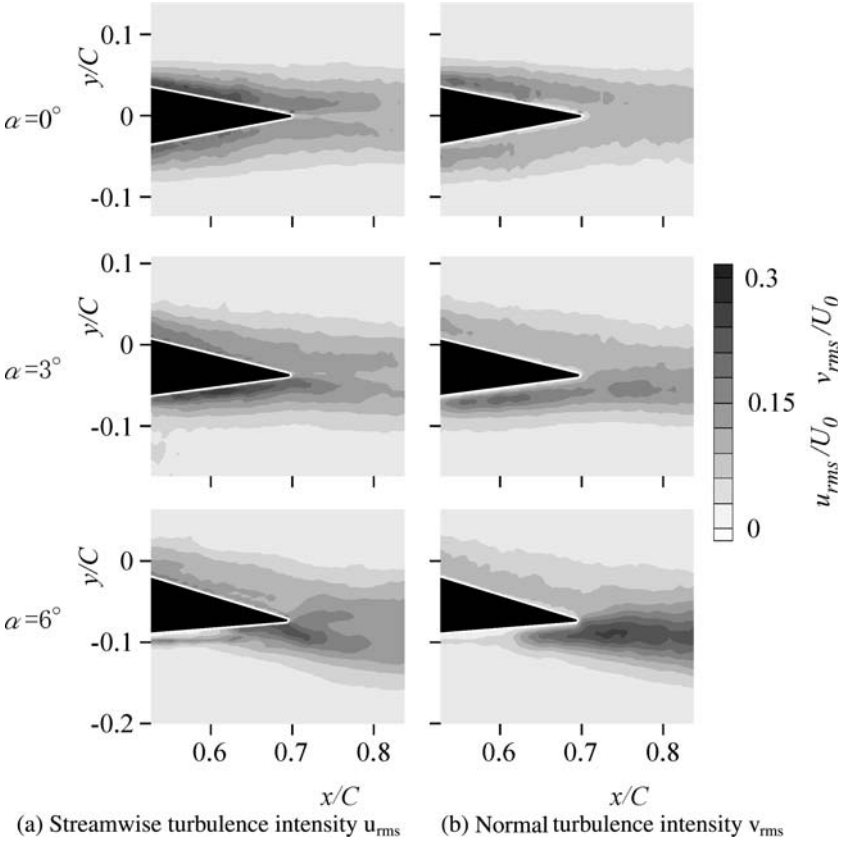

Fig. 9 Contour map of turbulence intensities: **a** Streamwise turbulence intensity u_{rms}, **b** Normal turbulence intensity v_{rms}

that the correlation peaks are distributed in a staggered arrangement, indicating that the vortex streets are generated along the separating shear-layer on the pressure surface. Note that the separation region was found at $X/C = 0.31$–0.65 on the pressure surface by liquid-crystal visualization (Nakano et al. 2002). With further increase in attack angle to 6°, highly periodical structure of correlation moves further downstream along the pressure surface toward the trailing edge of the airfoil. This is due to the downward movement of the separation region ($X/C = 0.4$–0.7) with an increase in attack angle to 6° (Nakano et al. 2002). On the other hand, the correlation contour on the suction surface is almost uniform at the attack angles 3° and 6°, which indicates that the flow structure on the suction surface is less related to the generation of tonal noise.

These features of correlation contour R_{up} are well reproduced in the contour map of R_{vp}. However, a line of peak correlation R_{vp} is formed along the mid height of the separating shear-layer over the pressure surface, indicating the formation of vortex structure along the pressure surface (Fig. 6c). It is found that the magnitude of cross-correlation R_{vp} is larger than that of R_{up}, which indicates a greater contribution of velocity fluctuation normal to the pressure surface on the formation of vortex structure.

Figure 8a, b show typical contour maps of instantaneous velocity fluctuations u' and v', respectively, at three attack angles 0°, 3°, and 6°. Note that instantaneous velocity fluctuations u' and v' directly contribute to the time-averaged cross-correlation contours R_{up} and R_{vp}. These contours indicates that the periodical structure of positive and negative correlation appears in the wake of the airfoil at attack angles 3° and 6°, as has been observed in the time-averaged cross-correlations in Fig. 7a, b. It should be mentioned that a similar magnitude of velocity fluctuation has also been generated in the flow field at zero attack angle and even on the suction surface at 3° and 6°, but they appear randomly in space. Therefore, the periodical structure cannot be generated in the wake of the airfoil at zero attack angle and on the suction surface at 3° and 6°, resulting in the removal of tonal noise as has been observed in the sound spectrum.

Figure 9a, b show typical contour maps of turbulence intensities u_{rms}/U_0 and v_{rms}/U_0 , respectively, at three attack angles 0°, 3°, and 6°. With an increase in attack angles, the turbulent region on the pressure surface becomes narrower than the suction surface, reflecting the movement of the reattachment point along the pressure surface. At the same time, the magnitude of turbulence intensities grows on the pressure surface in the near wake region. Therefore, the distribution of turbulence intensities in the near wake becomes asymmetrical about the airfoil axis. Note that the growth of turbulence intensities is larger on the normal component than on the streamwise component. These changes in the turbulence intensity distributions are similarly observed in the contour map of cross-correlation in Fig. 7, so that the growth of turbulence intensities in the near wake is due to the appearence of highly correlated structure of turbulence on the pressure surface of the airfoil.

5 Conclusions

The characteristics of tonal noise and the variations of flow structure of the NACA0018 airfoil are studied by using PIV measurement to understand the tonal noise mechanism. The measurements are made on the noise characteristics, the phase-averaged velocity field with respect to the noise signal and the cross-correlation contour of the velocity and the noise signal. The tonal noise is observed at small attack angles of the airfoil having a discrete frequency tone in the sound spectrum. The present experimental results indicate that the tonal noise source is distributed on the rear side of pressure surface and the periodic variations of velocity field are observed in the separating region on the pressure surface, which is followed by the upwash and downwash motion at the trailing edge of the airfoil. These flow phenomena over the airfoil surface result in the periodic formation of vortex streets in the wake of the airfoil. The tonal noise appears when the adverse pressure gradient on the pressure surface gets small enough to allow instability waves to grow slowly along the surface, scatter as sound when they are convected just past the trailing edge, so that the sound waves propagate upstream toward the boundary layer instability onset point, to initiate a feedback loop.

References

Akishita S (1986) Tone-like noise from an isolated two dimensional airfoil. AIAA paper, pp 86–1947

Arbey H, Bataille J (1983) Noise generated by airfoil profiles placed in a uniform laminar flow. J Fluid Mech 134:33–47

Fujisawa N, Hashizume Y (2001) Uncertainty analysis of temperature and velocity measured by liquid crystal visualization technique. Meas Sci Technol 12:1235–1242

Fujisawa N, Takeda G (2003) Flow control around a circular cylinder by internal acoustic excitation. J Fluids Struct 17(2003):903–913

Fujisawa N, Tanahashi S, Srinivas K (2005) Evaluation of pressure field and fluid forces on a circular cylinder with and without rotational oscillation using velocity data from PIV measurement. Meas Sci Technol 16:989–996

Hayashi H, Kodama Y, Fukano Y, Ikeda M (1995) Relationship between wake vortex formation and discrete frequency noise in NACA blades (in Japanese). Trans Jpn Soc Mech Eng 61(B):2109–2114

Howe MS (1978) A review of the theory of trailing-edge noise. J Sound Vib 61:437–465

Kim HJ, Lee S, Fujisawa N (2005) Numerical study on flow and noise characteristics of NACA0018 airfoil using large eddy simulation, Int J Heat Fluid Flow, in press

Kompenhans J, Raffel M, Dieterle L, Dewhirst T, Vollmers H, Ehrenfried K, Willert C, Pengel K, Kähler C, Schröder A, Ronneberger O (2000) Particle image velocimetry in aerodynamics; technology and applications in wind tunnels. J Vis 2:229–244

Longhouse RE (1977) Vortex shedding of low tip speed, axial flow fans. J Sound Vib 53:25–46

McAlpine A, Nash EC, Lowson MV (1999) On the generation of discrete frequency tones by the flow around an aerofoil. J Sound Vib 222:753–779

Manoha E, Troff B, Sagaut P (2000) Trailing-edge noise prediction using large-eddy simulation and acoustic analogy. AIAA J 38:575–583

Nakano T, Kim HJ, Lee S, Fujisawa N, Takagi Y (2002) A study on discrete frequency noise from a symmetrical airfoil in a uniform flow. In: 5th JSME-KSME Fluids Eng conference, Nagoya, Pa.OS6–2–4

Nash EC, Lowson MV, McAlpine A (1999) Boundary layer instability noise on airfoils. J Fluid Mech 382:27–61

Paterson RW, Vogt PG, Fink MR, Munch CL (1973) Vortex noise of isolated airfoils. J Aircraft 10:296–302

Raffel M, Willert CE, Kompenhans J (1998) Particle image velocimetry. Springer, Berlin Heidelberg New York, pp 147–171

Roger M, Moreau S (2004) Broadband self-noise from loaded fan blades. AIAA J 42:526–544

Shih C, Lourenco L, Krothapalli A (1995) Investigation of flow at leading and trailing edges of pitching-up airfoil. AIAA J 33:1369–1376

Tam CKW (1974) Discrete tones of isolated airfoils. J Acoust Soc Am 55:1173–1177

Tomimatsu S, Fujisawa N (2002) Measurement of aerodynamic noise and unsteady flow field around a symmetrical airfoil. J Vis 5:381–388

Wang M, Moin P (2000) Computation of trailing-edge flow and noise using large-eddy simulation. AIAA J 38:2201–2209

Wright SE (1976) The acoustic spectrum of axial flow machines. J Sound Vib 45:165–223